Automatic Image Analysis for Biomedical Research: Rapid Drug Susceptibility Testing and Investigation of Cell Specialization in Early Embryo

Grushnikov Andrey[1,a)]   Kanade Takeo[2]   Yagi Yasushi[1]

Abstract: Cell analysis is one of the core procedures done frequently during the course of research in a number of fields, including bacteriology and embryology. It is often done manually, examining images gathered with a microscope. This approach is labor-intensive and lacks reproducibility, emphasizing the importance of an automatic solution for the cell analysis problem. This work presents image processing based automation solutions for two cell analysis problems: drug susceptibility testing and early-stage embryo segmentation. The first problem we solved for a recently introduced device, by processing its images that contained cells. Cells were detected, their features extracted and used as input for SVM predicting drug susceptibility. The solution of the second problem involved applying 3D level set with custom energy functions for processing Z-stacks of fluorescence microscopy images. Both tasks were implemented as stand-alone tools, showed high accuracy on the respective datasets.

Keywords: medical image processing, classification, segmentation

1. Introduction

Analysis of visual data is the main procedure during the experimental stage of research in various fields, including biology and medicine. New devices for capturing images and advances in microscope design facilitated the acquisition of extremely large volumes of visual data. Not only improvements in hardware contributed towards the increase of data quantity, but also progress in developing novel techniques for visualization, for example, those that allowed to target and display particular parts of living cells and investigate the time-depended internal changes [1]. Despite an explosive increase in the rate at which digital image data is obtained in biological studies, the development of methods for its automatic processing and analysis is dramatically lacking [2].

There are a number of difficulties which prevent the adoption of existing image processing algorithms for numerous biomedical tasks. First, due to the substantial variety of images obtained in each particular task, it is nearly impossible to create a fully unified method, thus each time it is necessary to tune a previously introduced technique or develop one from scratch. Second, deep knowledge in both fields - computer science and biology - is required to construct an efficient algorithm, which can be achieved only by strong collaboration between researchers of different specialties. Finally, there is a necessity of constant maintenance, since the procedure of capturing data can change dramatically during the experimental stage.

An increasing number of studies have presented results of applying computational image processing methods to biomedical data [3], [4], [5], [6]. Yet, there is still a strong need for automated methods that are capable of conducting image analysis providing robust, accurate, objective metrics and alleviating specialists of labor-intensive work.

Investigation of cell morphology, growth, reaction to chemical agents is a frequently occurring problem in biomedical research. It is a core task in many different fields including bacteriology and embryology. Automation of this procedure is rather complicated since it often demands to conduct several procedures – perform cell detection, carry out tracking, extract a number of cell features, and provide a high-level judgment.

During the course of studies presented in this paper automatic solutions for two cell analysis problems have been constructed: rapid drug susceptibility testing and early-stage embryo segmentation.

2. Rapid drug susceptibility testing

A rapid increase of bacteria strains resistant to multiple drugs observed in recent years is a highly alarming issue [7]. Various factors contribute towards this tendency, among which inappropriate use of antibiotics in animal husbandry and overprescription of drugs are the most significant [8]. The development of new antibiotics is a costly procedure that requires investigation of genetic makeup of each individual bacteria strain and meticulous testing of a plethora of active chemical agents. The procedure of testing new potential active agents during clinical research is called drug susceptibility testing (DST).

[1]   Osaka University, Japan
[2]   Carnegie Mellon University
[a)]   andrey@am.sanken.osaka-u.ac.jp

2.1 DST

DST is the process of investigation bacteria strain resistance to different concentrations of various drugs. There are two types of DST: genotyopic that involves gene sequencing for identifyinbg mutated genes, and phenotypic that observes visual morphological changes in cells, directly examines responses to antimicrobial agents. Unlike genotypic, phenotypic primarily analyze visual information of the microorganisms inspecting replication of cells at different drug concentrations and comparing it with a reference control sample. The minimum concentration of a drug that prevents bacteria growth is referred as minimum inhibitory concentration (MIC).

Among the most common and wide spread methods for conducting DST is a microbroth dilution method [9], [10]. The DST procedure with this method starts with preparing two-fold dilutions of antibiotics in a liquid growth medium dispensed in test tubes. These test tubes assembled in trays, which often contain 96 wells, allowing to test approximately 12 different drugs in a range of 8 two-fold dilutions simultaneously. To cary out testing, drugs are pre-introduced and then a bacterial suspension is transfered into each well. The accuracy of the method is very high, and it is commonly used for obtaining ground truth MIC for bacteria strains. Alternative methods for performing DST are gradient and disk diffusion methods. These methods assess the susceptibility levels of bacteria cells by evaluating the shapes of an area free of bacteria cells formed as a result of the presence of antibiotic test strips or paper disks [11], [12]. The MIC in these techniques is determined after an overnight of incubation.

Several attempts to develeop a rapid and automized machines and methods for conducting DST have been done. For example, a MicroScan device capable of providing data after 22h was designed to incubate and analyze up to 96 microdilution trays [13]. The Vitek 2 System uses compact plastic reagent cards, that contain small quantities of an antibiotic and test media in a 64-well format. The device can be configured to perform up to 240 simultaneous tests, and collecting results after 4-10 hours of incubation. Despite several solutions for automation of DST procedure do exist, the high price of the devices and necessity to perform full-length incubation cycle of bacteria isolates restricts the wide spread of these systems. In rescently published works a number of new inexpensive devices and rapid DST techniques have been proposed [14], [15]. One of the proposed methods involves using the drug susceptibility testing microfluidic (DSTM) device designed by Matsumoto et al. [16], [17]. It was showed that this device can provide readable data in no more than 3 hours, quicker than the majority of other devices.

2.2 DSTM device

The DSTM device is prepared as follows. It contains five sets of four microfluidic channels, printed in a polymer on a cover glass [17] . Four channels in one set share inlet hole allowing to perform observations of cell growth with an introduced drug with three different concentrations and a control sample (see Figure 2).

The following procedures are conducted in order to determine MICs for bacteria strains using the DSTM device. First, a drug in different concentrations is introduced in three test microfluidic

channels of each one of the channel sets. The remaining channel is used as the control sample for the observations. Next, after the drug solution is dried, a cation-adjusted Mueller-Hinton broth of bacteria culture, grown in advance on Heart infusion agar, is introduced with a micropipette. Finally, the fully prepared device is incubated under humid conditions at 37°C for up to 3 hours.

The protocol of estimating the MIC with the DSTM device consists of visual inspections of images of channel sets taken with a camera attached to a microscope. Visible differences in cell morphology, or a number of cells between test sample, and the control sample signify that the input strain is susceptible to the used drug at a particular concentration. The minimum concentration of the drug to which the strain is susceptible constitutes its MIC.

The growth rate of each individual bacteria strain can differ from other strains. Thus, it is not possible to carry out the comparison of the changes using a uniform control sample for all range of strains. Hence, the control sample of each strain must be incubated together with the test samples to perform correct observations.

Manual measurements of cell characteristics based on visual inspections were extremely labor-intensive, time-consuming, suffer from approach subjective biases and lack of reproducibility. To resolve this issue we developed an algorithm and implemented it as an automatic tool able to extract bacteria cell features as well as determine the susceptibility of a bacteria strain.
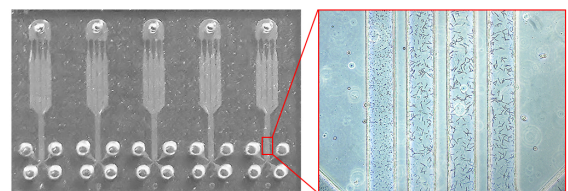
Fig. 1 An actual of the DSTM device, together with a microscopy image of the microfluidic channels.

## 2.3 Methods for cell analysis

A number of methods able to perform cell detection, tracking, and analysis have been introduced in recent years. A CellProfiler system is capable of simultaneously measuring size, shape, intensity, and texture of a variety of cell types in a high throughput manner [18]. After carrying out illumination correction, identifying cells with fluorescence markers it then measures a large number of simple and complex features for each cell. The calculated features include area, shape, intensity, texture, Zernike shape, Haarlick and Gabor texture features. Another automated cell analysis framework CellScreen was developed for automated quantification non-invasive cell counts in small volume cultivation vessels [3]. The system consists of an inverse microscope, equipped with a 10x lens, a camera, and a special application software. Initially, 96 well plate, filled with cell suspension is positioned on the motor stage, positioned and calibrated automatically. The images captured at the base of the well, then the number of viable and dead cells and their morphology is evaluated.

To solve the task of measuring strain susceptibility from an image of DSTM device, the existing methods require significant

modification. Different packages must be used at different stages of analysis, resulting in a complex workflow and an increased processing time. Therefore, the aim of the research was to develop a dedicated method for automatic processing microscopy images of DSTM device for performing DST.

2.4 Automatic DST with DSTM device

The developed algorithm for quantitative analyses and susceptibility assessment of a bacterial strain from an image of the DSTM device has five stages: noise reduction, localization of the channel regions, cell detection, feature extraction, susceptibility, and MIC estimation.
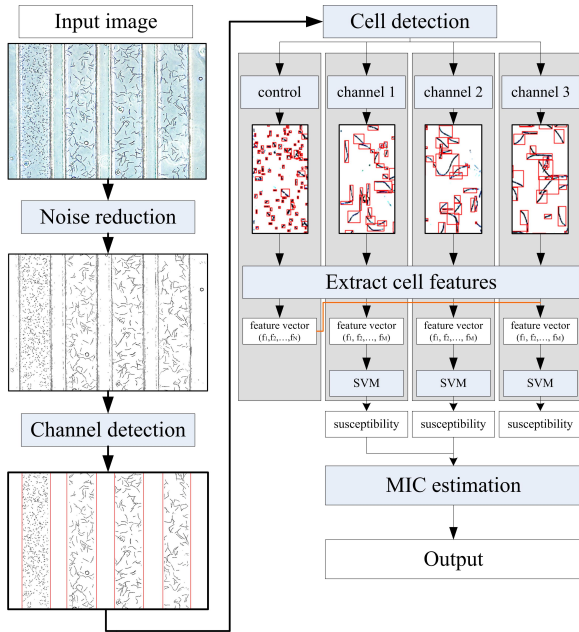
Fig. 2 A scheme of the proposed algorithm for processing an input image of DSTM device channel to extract cell features, estimate susceptibile for each drug concentration and obtain MIC

The input images are taken with a camera attached to a microscope. At the first stage, these images are enhanced by applying illumination correction and denoising. Next, Probabilistic Hough Transform is used to determine the borders of each individual microfluidic channel. At the following stage, a cell detection is carried out assigning a background or cell label for each pixel. The acquired segmentation facilitates the extraction of a various cell features, which are then normalized with those obtained from the control sample. The features are assembled into vectors, that serve as input for a pre-trained SVM, which determines if the bacteria strain is susceptible to a particular drug concentration or not. The least concentration of the drug for which the SVM predicted susceptibility is the MIC.

2.4.1 Illumination correction

The process of capturing digital images using microscopy often results in nonuniform illumination of the scene. For further correct processing of the visual data it is essential to enhance the image by performing illumination calibration. The illumination of image taken with a light microscope can be model to be guadratic using the following equation [19].
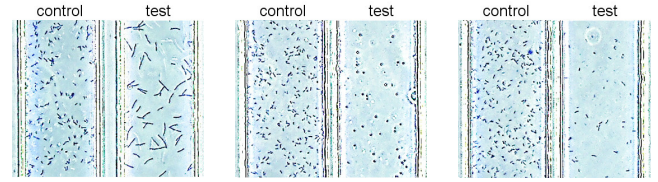
Fig. 3 Photographs of DSTM device channels illustrating cell responses to different antimicrobial agents: (a) cell elongation for ciprofloxacin, meropenem, piperacillin; (b) decrease in the number of living cells for amikacin; (c) formation of spheroplasts for meropenem.

$$I_q(x, y) = a_1 x^2 + a_2 y^2 + a_3 xy + a_4 x + a_5 y + a_6 \qquad (1)$$

The procedure for illumination correction minimizes and optimization function χ^2 based on least-squares estimators to fit it to the intensity distribution of the input image.

$$\chi^2 = \sum_{m=1}^{M} \sum_{n=1}^{N} (I(m, n) - I_q(m, n))^2 \qquad (2)$$

This illumination correction approach was directly applied to the input images of the DSTM device. It was followed by the binarisation procedure carried by Otsu adaptive thresholding [20]. This procedure separates foreground and background pixels to calculate threshold t by minimizing the weighted within-class variance of each type of pixels.

$$\sigma_w^2(t) = q_1(t)\sigma_1^2(t) + q_2(t)\sigma_2^2(t) \qquad (3)$$

2.4.2 Channel detection

The next step of the algorithm is the detection of DSTM device microfluidic channels in the input image. This is carried out by locating left and rights borders for each channel. The DSTM device is placed manually in the observation field, the position of the borders varies from image to image. Thus a dynamic algorithm for detecting these borders was constructed. It utilized Canny edge detection followed by Progressive Probabilistic Hough Transform (PPHT) [21]. The output of the PPHT is a set of lines – channel border candidates. Using additional constraints - generally vertical orientation of the lines and equality of channel widths.

2.4.3 Cell detection

Cell detection is the most challenging step in image analysis and its accuracy determines the efficiency of the resulting cell measurements.

A number of susceptible bacteria strains growing in the presence of a drug demonstrate anomalous growth, where cells do not divide and continue to elongate. At the captured image these cells appear as cluttered together, entangled, and overlapped. This issue had to be addressed to obtain the accurate number of cells present in each channel.

Watershed or level set techniques were not applicable for solving this problem due to the small scale of the cells [24]. Instead, a separation algorithm modeling overlapped cells as graphs and performing splitting was developed. At first, the algorithm extracts all connected regions using connected-component labeling method [25] applying it to the binary image obtained as the result of procedures carried out at the illumination correction stage. Next, morphological thinning is applied to using the Zhang-Suen method [26]. For each pixel, this method checks neighbors and

removes pixels if they correspond to a certain pattern. Thinning produces a skeleton representation of the original structure in which the intersection points are pixels two or more non-background neighbors. In addition to intersections, points where potential cells touch is located – points where the second derivative, violates the constraint, defined by a threshold constant.

At the next step, each cell is modeled as a graph that preserves its morphological structure. Intersection, endpoints and touch points become nodes, while the connection between these points become edges. All possible routes in the graph are extracted using the breadth-first search. For each route, smoothness constraint is checked and if it is not satisfied the route is removed from the set. The smoothness constraint is defined as the maximum allowed angle between nodes. A set of routes with the maximum number of nodes to cover the entire graph is chosen. The found routes represent individual cells and labeled accordingly. Finally, labels are assigned to pixels that were removed at the thinning stage.

2.4.4 Feature extraction

The output of the cell detection stage is a set of labeled pixels, which describes bacteria cells. From this data extracting a variety of different features to represent changes in cell growth is a fairly straightforward task.

Cell morphology is one of the major indicators of the strain sensitivity. To represent this attribute for each cell its area and length are calculated. The area is defined as the total number of pixels, while the length is approximated as the number of pixels in the thinned representation of the cell. Statistics of these two features, mean, minimum, and maximum, as well as an 8-bin histogram of cell frequencies in relation to length, are used to characterize strain growth in the presence of a particular drug concentration. In addition to shape features, the cell count is also added to the set of features to represent the number of the living cells.

The growth rate of bacteria strains varies significantly – two bacteria strains, obtained from different patients, could show completely distinct growth rates, even without the presence of a drug. Hence, to be able to compare cell characteristics of various strains the calculated attributes has to be normalized. This is done by dividing obtained variables from each one of three test channels by those calculated for the control channel, producing a set of relative attributes.

2.4.5 Susceptibility estimation

The prediction of susceptibility from a set of relative features for each microfluidic channel performed with a Support Vector Machine. Support Vector Machine (SVM) is a widely used supervised learning technique for classification and regression [27], [28]. Let set $X = \{(\vec{x_i}, y_i), i = 1, ..., N;\}$ be the training data where $\vec{x_i} \in R^d$ represents feature vectors and $y_i \in \{-1, 1\}$ are labels. SVM solves the classification problem by identifying a hyperplane, separating two classes. The task or building the separating hyperplane can be reformulated as a problem of solving a task of maximizing a Lagrangian L_D subject to additional constraints.

$$L_D = \sum_{i=1}^{N} \alpha_i - \frac{1}{2} \sum_{i=1}^{N} \sum_{j=1}^{N} \alpha_i \alpha_j y_i y_j \vec{x_i} \cdot \vec{x_j} \qquad (4)$$

$$\sum_{i=1}^{N} \alpha_i y_i = 0, \quad 0 \leq \alpha_i \leq C \qquad (5)$$

2.5 Experimental results
2.5.1 Dataset

The DSTM device used in the studies was prepared by fabricating microfluidic channels (width, $100\mu m$; height, $50\ \mu m$) in a polymer (polydimethylsiloxane - PDMS; Silpot184, Dow Corning Toray Co., Ltd., Tokyo, Japan) on a glass cover (Matsunami Glass Ind., Ltd., Osaka, Japan) using soft lithography technique [22]. The input images were captured with a USB camera, attached to a phase contrast microscope with 10-fold objective lens with JPEG compression and 1280x1024 resolution.

Five different drugs were applied to the bacteria strains: amikacin (AMK; Nichi-Iko Pharmaceutical Co., Ltd. Toyama, Japan), ciprofloxacin (CIP; Meiji Seika Kaisha, Ltd., Tokyo, Japan), meropenem (MPM; Meiji Seika Kaisha, Ltd.), ceftazidime (CAZ; Sawai Pharmaceutical Co., Ltd, Osaka, Japan), piperacillin (PPC; TOYAMA CHEMICAL CO., LTD, Tokyo, Japan). Each one of the drugs was used in three different concentrations during the testing phase: AMK (4, 8 and 16 mg/L), CIP (1, 2 and 4 mg/L), MPM (1, 2 and 4 mg/L), CAZ (4, 8 and 16 mg/L) and PPC (4, 8 and 16 mg/L). The active agents were dissolved in water, injected into microfluidic channels, and then freeze-dried before using the DSTM device [23].

Strains of 101 clinically isolated bacteria specimens of *Pseudomonas aeruginosa* ATCC27853 were used in experiments. The strains were grown overnight on Heart infusion agar and suspended in cation-adjusted MuellerHinton broth, and then were introduced with a micropipette into the DSTM devices. Next, the DSTM devices then were incubated under humid conditions (37C) for up to 3h. The ground truth MICs were determined for the same set of bacteria strains with the microbroth dilution method [9], [10].

#### 2.5.2 Channel and cell detection accuracy

The first set of the experiments aimed to determine the of the channel detection stage of the algorithm. Since each image contained 4 channels, and the number of images was 505 (101 images per each drug), the total number of channels to detected was 2020. Among these only 8 were not correctly detected, due to less prominent channel borders.

Next, it was necessary to evaluate how well the designed algorithm is able to locate cells. It was not possible to generate a ground truth segmentation by manually labeling each pixel as belonging to an individual cell or background due to the number of cells and images. In addition, no automatic method would be able to resolve this issue. Therefore, to conduct estimation of cell detection accuracy, the cells in 100 sample channels from 25 randomly chosen images were manually counted. Then, the obtained values were compared with those calculated by the proposed technique.

The figure 4 displays are scatter plot that represents the relationship between the number of cells identified automatically

with those counted manually. The average accuracy of correctly detected cells was 93%. Careful analysis of the samples where misdetection had occurred revealed that the main cause of errors is highly overlapped elongated cells where the algorithm labels segments as individual cells.
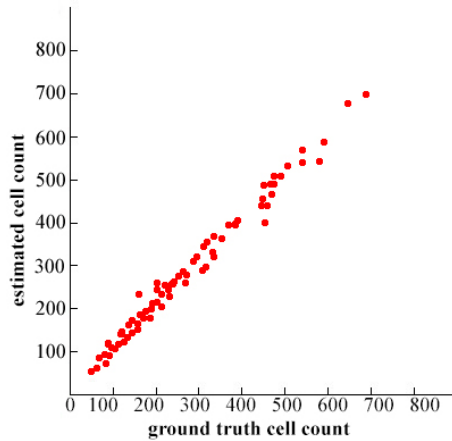
Fig. 4 Scatter plot that represents the accuracy of cell detection with the proposed algorithm.

2.5.3 Susceptibility estimation

Evaluation of the susceptibility estimation accuracy was one of the main targets during the experimental stage. The entire dataset containing 303 feature vectors (3 test samples for each one of 101 images) was split into training and testing sets in the ratio 80:20 and testing were done with cross-validation. Separate SVMs were trained for each individual antimicrobial agent.

Several feature vectors for SVM training was combined with different cell characteristics to investigate which set of features is able to achieve the highest accuracy. The following feature sets were used: (F1) length statistics, (F2) area statistics, (F3) count and average length, (F4) count and average area, (F5) average length and area, (F6) histogram (see Table 1).

Feature	Drug				
	AMK	CIP	MPM	CAZ	PPC
ALL	**0.91**	**0.96**	**0.94**	**0.95**	**0.9**
F_1	0.81	0.85	0.9	0.88	0.89
F_2	0.83	0.88	0.89	0.86	0.87
F_3	**0.9**	**0.96**	**0.94**	**0.94**	**0.9**
F_4	0.85	0.88	0.87	0.85	0.88
F_5	0.78	0.83	0.87	0.87	0.89
F_6	0.89	0.95	0.94	0.92	0.9

Table 1 Susceptibility estimation accuracies for feature vectors constructed from different cell characteristics

For CAZ and PPC, features indicating length (F3, F4, and F5) were more reliable characteristics for estimation, whereas for AMK and CIP it was cell count. For MPM, feature vectors indicating length or cell count were equally accurate. The average accuracy of susceptibility estimating exceeded 90%.

2.5.4 Susceptibility estimation: 2h vs 3h incubation

Above it was shown that the developed algorithm is capable of estimating strain susceptibility with a rather high accuracy after 3h of incubation. Since it is important for bacteriologists to obtain results as soon as possible, we aimed to investigate how well the SVM can predict susceptibility from images taken earlier than 3h.

The same dataset of 101 strains and 5 drugs was used during this experiment, yet the input images were captured merely after 2h of incubation. The feature vectors fed into the SVM consisted of only two elements: cell count and average length. Then, the accuracy of susceptibility estimation after 2h for each drug was compared with the one, achieved after 3h. The results of this examination is presented in Table 3.

Incubation time	Drug				
	AMK	CIP	MPM	CAZ	PPC
2 h	0.74	0.85	0.82	0.8	0.79
3 h	0.9	0.96	0.94	0.94	0.9

Table 2 Susceptibility estimation accuracy using a feature vector, reflecting only cell count and average length, on samples incubated for 2 h or 3 h

After 2h of incubation, the difference between cell features of the control and test samples the accuracy of susceptibility estimation was dramatically lower. The minimum value was of 74% was observed for the amikacin (AMK). The explanation of this fact is that the bacteria strains grown in the presence of AMK expressed lesser morphological changes in comparison to other drugs.

2.5.5 MIC estimation accuracy

To provide more statistics for evaluation of the developed method the degree of correlation between predicted MIC and the ground truth was calculated. To get the estimation of the minimum concentration for each individual bacteria strain, the susceptibility of each channel in the corresponding image was calculated with the pre-trained SVM from a feature vector, containing only cell count and average length. Then, the MIC was assigned as the minimum concentration among susceptible channels. The ground truth MIC was obtained by applying the microbroth dilution method using the same bacterial solution on the same day.

Including samples that showed a two-fold difference in the MIC, as determined by the traditional microbroth dilution method, the matching rate of the proposed method was at least 96% (see Table 3).

	Drug				
	AMK	CIP	MPM	CAZ	PPC
Accuracy	0.97	0.99	0.97	0.97	0.96

Table 3 Accuracy of MIC estimation for different drugs based on a feature vector containing only cell count and average length.

2.5.6 SVM classifier vs human export

The final set of experiments was dedicated to comparing the accuracy of MIC prediction with the SVM with the criteria devised by a human expert, that investigated various features: length, count, the ratio of cell pixels to the background, and distribution of cells with different lengths. The criteria proposed by the expert were derived obtain through trial and error to represent the best correlation between estimated and ground truth MICs **?**.

2.6 Implementation

The goal of the conducted study was not only to design an algorithm for automatic analysis of input images of the DSTM device but also to develop a stand-alone software tool, that could

	Drug				
	AMK	CIP	MPM	CAZ	PPC
SVM	0.97	0.99	0.97	0.97	0.96
Human	0.96	1.0	0.97	0.97	0.96

Table 4 MIC estimation with the trained SVM classifier vs criterie selected by a human expert

be used not only by highly skilled experts but also by those who don't have significant knowledge in the field of bacteriology. The implemented tool was designed to have a GUI to provide users with a simple way for conducting the analysis. The tool is capable of processing a single image as well as multiple images in a batch manner (see Figure 5).

The processing speed of the implementation was evaluated using a machine that had the following characteristics: Intel Core i7-6700K, 4.0 GHz, 32 GB RAM. Since the cell detection step of the algorithm can be carried out independently for each channel, a parallel procedure using thread technology has been implemented.

The speed of processing varied, increasing the number of cells. Yet it did not exceed half a minute for a single input image. The longest time was observed for channels with highly overlapped samples (see Table 5).

Cell count	100	300	600
Without overlapped cells	11s	15s	22s
With overlapped cells	12s	17s	35s

Table 5 Processing speed, given in seconds, of the implemented algorithm for different average number of cells in a single channel.

2.7 Comparison with existing DST methods

Previously, the methods for conducting DST to produce visual differences in growth between control and test samples required long incubation times. Advancements in nanotechnology allowed to rely on microfluidic chips and microscopy for a wide range of microbiological experiments [16].

Among all proposed procedures for DST, only a handful was able to obtain results in less than 4h. For example, Choi J. et al. [29] described a method involving microfluidic agarose channel chip for MIC acquisition by analyzing alterations in bacterial number and size occurred in response to drugs. The method required a complicated process of setting up a 96-well type unique plate and conducting observations where images of the plate had to be taken one by one at a certain time interval.

Other approaches were focused on designing microfluidic chips and measure susceptibility by assessing time-lapse images [30], [31]. Notably, Price et al. [32] using an automated microscopy system analyzed susceptibility of *Staphylococcus aureus* obtaining results in 2-4h. The approach required 2h preincubation to get logarithmically growing cells, yet was not suitable to assay multiple strains simultaneously.

The key factor that contributed to the rapidity of susceptibility estimation with the DSTM device is the introduction of a microscope. The damaged bacteria cells treated by antimicrobial agents are easily visualized with a microscope. In comparison to other methods, to obtain visual information with the DSTM device requires less than 4 hours: 10 min to set-up and 3h of incubation.

The algorithm developed for automatic cell detection facilitates the analysis of bacteria cells, and capable of processing input images within 2 minutes. The advantage of the automatization is not only the speed of result acquisition but also the accuracy of cell detection, susceptibility estimation, and MIC prediction, that was proved with the conducted experiments to be similar to a highly skilled expert [33].

The implementation of the algorithm as a stand-alone software tool was deemed useful to bacteriologist in daily research since it provided an easy to use graphical interface and functionality to extract cell features for more detailed analysis.

It is planned to expand the range of bacteria types for which the method can be applied, and propose to use the DSTM device in daily tests in hospitals. The implementation of the developed automatic algorithm for susceptibility testing will be supplied with the device. When this technology is put into practical use, susceptibility testing will elevate the need for expensive equipment providing low cost, simple, accurate and rapid tool.
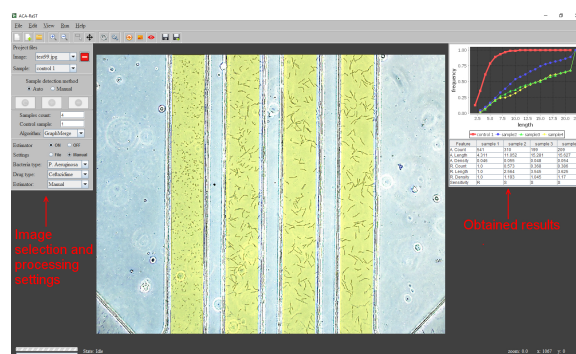
Fig. 5 A screenshot of the graphical interface of the developed software applications. The menu panels on the left side of the application allow to choose imported images, manually select channel areas, and specify processing parameters. The central area is designated for displaying input and processed images. The panel of the right displays a frequency chart and cell characteristics.

3. Early stage embryo segmentation

3.1 Cell analysis in embryology

Embryology is a wide field of study that includes investigation of internal mechanisms of a variety of processes that occur in a developing embryo. The early stages of growth, from fertilization to implantation, are of particular interest to the medical community. Advances in molecular biology and microscopy provided new insights into what is taking place at these stages of embryo development.

The development of the pre-implantation embryo starts from a single fertilized cell, the zygote. The first division of the zygote usually occurs within 24 hours after ovulation and produces two cells – blastomeres. Subsequently, a series of mitotic divisions take place, yet the volume of the embryo remains constant, while the newly formed blastomeres become smaller and smaller. When the number of cells reaches 16 the embryo enters the morula stage, during which identical blastomeres start to differentiate to give rise to different types of cells in the body [34], [35]. Blastomeres extracted from an embryo are called embryonic stem cells. These cells became known for their ability to

proliferate and replicate themselves indefinitely and yet maintain the developmental potential to form any cell type. This unique feature promises to establish new efficient transplantation treatments for regenerative medicine. Yet to fully unlock the potential of these cells a detailed model that describes the specialization process is required.
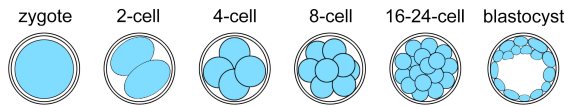
Fig. 6 Overview of the pre-implantation development of a mouse embryo during which a fertilized egg divides into increasingly smaller cells resulting in the formation of the blastocyst.

A number of hypotheses have been proposed to explain the process that drives cells to commit to a distinctive line. Early ones were based on assumptions that development of an embryo was driven by random processes, where cell contributed equally to any type of lineage. However, more recent time-lapse imaging studies suggest that a variety morphological characteristic - volume, shape and relative positions of blastomeres - play a significant role in determining cell fate [36], [37], [38]. Despite significant progress in understanding the process of cell specification, there are other aspects that also contribute to the determination of the resulting cell [39], [40].

Uncovering all the mechanisms, underlying the specification of individual cells and establishing a complete model, requires quantitative analyses of various blastomere characteristics. They can be obtained without a considerable effort if segmentation into individual cells is performed. A number of methods to automate this labor-intensive procedure have been developed over the past decade.

3.1.1 Methods for blastomere segmentation

Embryos are commonly imaged by means of phase contrast technique called Hoffman Modulation Contrast (HMC). This approach converts optical gradients into variations of light. Obtained HMC images display a transparent embryo with a side-lit appearance.

Singh et al. [41] presented a segmentation algorithm for processing a single HMC image for estimating embryo viability for fertility. The algorithm successfully segments up to 4 blastomeres, applying isoperimetric graph partitioning, followed by region merging which uses length, vesselness, and entropy of the borders between regions. To estimate shape, least-squared fitting of an ellipsoidal model is used. For the task of performing 3D morphology measurements and modeling of an embryoGuisti et al. [42] presented a graphcut-like global energy minimization approach for segmenting a Z-stack of HMC images and extracting 3D morphology characteristics from HMC images are captured at different focus levels.

Graphcut-based algorithms, being very versatile, showed efficiency in segmenting each individual cell nuclei in histopathology images and tissue samples of higher organisms [43]. The watershed approaches described in [44], [45] were also able to successfully detect nuclei in tissue or cell cultures. Segmentation by gradient vector flow tracking was capable of producing

accurate results, however, it is sensitive to object texture.

Another technique that showed efficiency on a dataset containing microscopic images of 381 8-cell embryo was proposed by Tian et al. [46]. The method is based on least square curve fitting applied to phase contrast image to detect blastomeres. Then the method used edge detection, removing of multiple connected points and morphology operations to obtain part of cell edges.

3.1.2 Embryo segmentation from fluorescence images

Embryonic development is a dynamic three-dimensional process of complex cellular interactions. For high-resolution visualization of development progression genetically encoded fluorescent protein (FP) reporters have been most prominent, because of their high signal-to-noise ratio, minimal toxicity, and ease of use [47]. There are various methods for visualizing FP reporters. Widefield fluorescence microscopy for observing whole embryos, confocal microscopy that allows visualizing an embryo at subcellular and spatiotemporal resolution, and light sheet fluorescence microscopy, that utilizes plane of light to optically section and view tissues with subcellular resolution.

Unlike segmentation, an embryo from HMC images, techniques that provided similar output for fluorescence microscopy images has not been well studied. Nevertheless, a number of algorithms for general cell segmentation in fluorescence images have been developed [5], [6], [48].

Dufour et. al [5] proposed a method, based on multiple active surfaces, for automatic segmentation and tracking fluorescent cells in 3D microscopy. The algorithm is able to process multiple cells, even if they touch, divide or move. An improved version of this method, in terms of tracking precision and computational time, was introduced by Dzyubachyk et. al [6]. Xinghua et al. [48] developed a tool designed to provide quantitative cells measurements in fluorescent intensity 2D and 3D image data. The main algorithm consists of a detection module to identify each nucleus, a segmentation module that propagates assigned labels to the entire body of the respective nucleus, and a classification module identifying different types of cells.
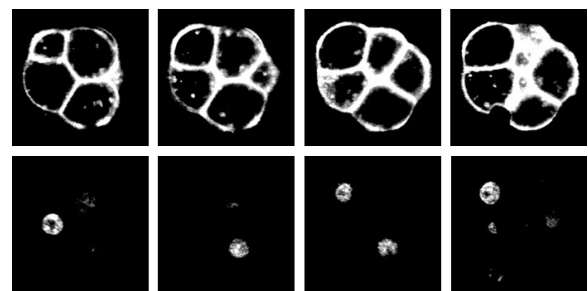
Fig. 7 Cross sections images of an 8 cell embryo nuclei and membranes. To mark nuclei and membranes H2B-mCherry and mG proteins were used.

Inspired by achievements of these works in applying level set based techniques for segmentation and tracking cell the aim of our studies was to design and implement a new level set approach for the task of segmentation early stage embryo in fluorescence images. The input images were obtained by first, applying excitation light to embryos obtained by crossing female H2B-mCherry mice with male mG mice [49] (see Figure 7). Then, cross sections

of the embryos were captured with a light microscope resulting in two Z-stacks of 3D fluorescence microscopy images: one stack of cell nuclei and another one of membranes. The segmentation task is formulated as the detection of inner regions for each individual cell as well as localizing the whole volume, occupied by membranes (see Figure 8). Membranes, corresponding to individual cells can be afterward acquired from the solution by locating surfaces equidistant from inner cell region boundaries with the distance transform [50].
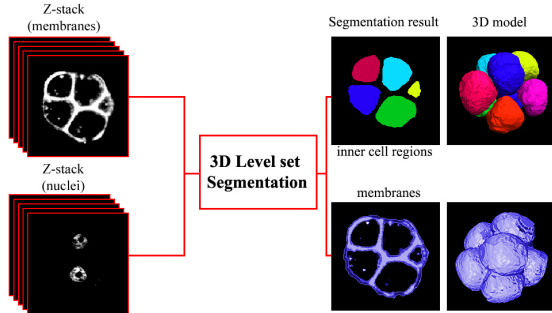
Fig. 8 To perform segmentation of an embryo 3D level set method is applied to two Z-stacks of fluorescence microscopy images. One of the Z-stacks composed of images displaying cell membranes, while the other one contains visual information about cell nuclei positions.

3.1.3 3D level set segmentation

The segmentation task can be solved with different methods. Filtering techniques, for example, Canny edge detector, rely only on local information and don't guarantee continuously closed edge contours. Snake [51] and Balloon [52] methods require good initial estimation of the region boundaries and use edge cues to carry out segmentation, however, they lack a meaningful probabilistic interpretation and global conditions. Learning based algorithms are capable of achieving high segmentation accuracy, yet they require a considerable amount of input data to train on. Finally, optimization techniques based on energy functions or Bayesian criteria involve the usage of global criteria for which solving a minimization task is difficult.

A trade-off between local and global criteria is the level set method [54]. It performs evolution by fitting statistical models to intensity, color or texture with each of the separated regions. The advantages of this technique are less sensitive to noise and to varying initialization, ability to handle complex morphology and topological changes automatically. The major drawback of the method, however, is that solving the defined partial differential equation (PDE) is often computationally expensive. This issue is commonly overcome by limiting the region where computation is performed [53] or totally avoiding solving the PDE [55].

To estimate cell membranes correctly, instead of directly attempting to locate each one of them individually the developed algorithm performs segmentation into inner cell regions and the whole region occupied by membranes. For each type of object to segment, a separate level set energy function as a differential equation was defined that penalizes overlapping with other segments, forces membrane to wrap around inner regions, and specifies that inner cell boundary is where intensity changes significantly.

The level set method was introduced in [54] to track moving interfaces for various problems in fluid dynamics. Later it was successfully applied to perform segmentation in computer vision. The central idea behind this method is to evolve the boundary surface S in the domain $\Omega \in R^3$ from some initialization in direction of negative energy gradient with the gradient descent procedure presented in the equation (6).

$$\frac{\partial S}{\partial t} = -\frac{E(S)}{S} = F \cdot n \qquad (6)$$

$$\frac{\partial \phi}{\partial t} = -\frac{\partial E(\phi)}{\partial \phi} = -F|\nabla \phi| \qquad (7)$$

Following the approach for identifying multiple segmentation regions [56], individual level set functions ϕ_i are defined for each of N inner cell region boundaries and one ψ is set to describe the surface of the membranes, all of which are evolved simultaneously.

3.1.4 Energy functions

The choice of the energy function $E(\phi)$ is important, since it determines the accuracy and robustness of the level set method. In the developed approach individual energies $E_{inner}(\phi_i)$ and $E_{membrane}(\psi)$ were constructed for the two types of level set functions ϕ_i and ψ respectively.

3.1.4.1 Inner region energy

The inner region energy $E_{inner}(\phi_i)$ is designed to describe the morphology of the inner cell region boundary. It is a weighted sum of four terms.

$$E_{inner}(\phi_i) = w_1 E_{edge}(\phi_i) + w_2 E_{nucleus}(\phi_i) + w_3 E_{overlap}(\phi_i) \qquad (8)$$

The edge energy $E_{edge}(\phi_i)$ measures how well the surface S_i matches the boundary of the $i-th$ cell inner region. It is defined following the approach of geodesic active contours.

$$E_{edge}(\phi_i) = \iint_{S_i} e(x, y, z) \, ds \qquad (9)$$

In the equation above, function $e(x, y, z)$ is the edgeness metric. It can be defined with a number of methods, however, for any definition, the function must be zero at the boundary surface of a segmented object and take large values elsewhere. In the proposed approach the edgeness metric was specified as the Euclidean distance from each point of the detected surface S_i to the cell membranes displayed in fluorescence images.

The energy $E_{nucleus}(\phi_i)$ characterizes the position of the nucleus, forcing the inner region to contain nuclei inside it.

$$E_{nucleus}(\phi_i) = -\iiint_{Q_i} \log p(Q_i|I(\vec{x})) dx \, dy \, dz - \\ \iiint_{Q_0} \log p(Q_0|I(\vec{x})) \, dx \, dy \, dz \qquad (10)$$

The $I(\vec{x}) = I(x, y, z)$ is the intensity of the pixel (x, y) in the $z-th$ cross section of the nuclei z-stack. The Q_i denotes the region occupied by the $i-th$ nucleus, while the Q_0 is the background.

The terms $\log p(Q_i|I(\vec{x}))$ and $\log p(Q_0|I(\vec{x}))$ represent logarithm of posterior probabilities of a pixel (x, y, z) to belong to the inner cell region or background, depending on its intensity $I(\vec{x})$.

The surface boundaries of the all individual cell membranes combined together are specified by the energy $E_{membrane}(\psi)$. It consists of three terms: one that specifies occupied volume that depends on the intensity of voxels in fluorescence images of membranes, other penalizes overlapping with inner cell regions and the final one, that prevents occurring tearing in the surface by attempting to cover inner cell regions.

$$E_{membrane}(\psi) = v_1 E_{volume}(\psi) + v_2 E_{overlap}(\psi) + v_3 E_{inclusion}(\psi)$$
$$(11)$$

$$E_{volume}(\psi) = - \iiint\limits_{\Omega_1} \log p(\Omega_1|J(\vec{x})) \, dx \, dy \, dz -$$
$$- \iiint\limits_{\Omega_0} \log p(\Omega_0|J(\vec{x})) \, dx \, dy \, dz \quad (12)$$

The components Ω_1 and Ω_0 correspond to membranes region and the background respectively. The $J(\vec{x}) = J(x, y, z)$ is the intensity of the membrane pixel (x, y, z).

The energy function $E_{overlap}(\psi)$ is constructed similar to $E_{overlap}(\phi_i)$ penalizes the membrane overlap with cell inner regions.

$$E_{overlap}(\psi) = \sum_i \iiint\limits_{\Omega_1} H(-\psi(\vec{x})) H(-\phi_i(\vec{x})) \, dx \, dy \, dz \quad (13)$$

The fluorescent proteins mark cell membranes nonuniformly, which makes some images display nonexistent holes in membrane surface. To overcome this issue and restore the correct structure of the embryo the term $E_{inclusion}(\psi)$ was designed to force the membrane to cover inner cell region.

$$E_{inclusion}(\psi) = \iiint\limits_{\Omega_1} \frac{1}{1 + e^{(k*(d(x,y,z)-D))}} \, dx \, dy \, dz \quad (14)$$

The function $d(x, y, z)$ measures the distance from the point (x, y, z) to the boundary of the inner cell region. The constant D sets the maximum allowed distance from the membrane to the inner cell regions.

To summarize all the above, for the segmentation problem defined as locating inner cell regions and membranes it is necessary to solve $N + 1$ PDEs, where N is the number of cells in the embryo.

$$\frac{\partial \phi_i}{\partial t} = -\frac{\partial E_{inner}(\phi_i)}{\partial \phi_i} = -F_{inner}|\nabla \phi_i|, \; i = \overline{1, N} \quad (15)$$

$$\frac{\partial \psi}{\partial t} = -\frac{\partial E_{membrane}(\psi)}{\partial \psi} = -F_{membrane}|\nabla \psi| \quad (16)$$

It has to be noted that these equations are mutually dependent due to energy functions $E_{inner}(\phi_i)$ interact with each other and with the $E_{membrane}(\psi)$ via the $E_{overlap}(\phi_i)$ and $E_{overlap}(\psi)$. Thus the equations (15) and (16) have to be solved simultaneously.

3.1.5 Fast two cycle level set

Direct implementation of the level set method has a major drawback: directly and fully solving PDEs defined by equations (15) and (16) with numerical methods is computationally expensive. To increase the processing speed a number of techniques were proposed. Some methods were focused on updating the level-set function globally over the entire regular grid, while others performed computations only in a restricted neighborhood of the zero level set. The later approaches are called narrowband techniques [57], [55].

One example of narrowband methods is [57], where a tube is constructed in the neighborhood of the zero level set, that is initialized as a signed distance function within this tube. When the zero level set becomes too close to the edge of the tube, then both the tube and level set function is reinitialized with the fast marching method.

A significant number of development methods attempt to solve the associated evolution PDEs accurately, yet for some problems, such as image segmentation, accuracy is not necessary. Exploiting this idea Shi and Karl [55] developed a method, that completely avoids direct calculations of PDEs. This method was able to achieve near real-time performance due to the fact that it does not demand reinitialization of the level set functions and update it only in the narrow band.

The boundary surface in the level set method is defined via the zero level set function ϕ that in discrete case is defined over a grid. Specifying that ϕ is negative inside the and positive outside the surface with the implicit boundary representation, it is possible to define two sets L_{in} and L_{out} of neighboring points.

$$L_{in} = \{\vec{x}|\phi(\vec{x}) < 0, \exists \, \vec{x}_0 \in N(\vec{x}) : \phi(\vec{x}_0) > 0\}$$
$$L_{out} = \{\vec{x}|\phi(\vec{x}) > 0, \exists \, \vec{x}_0 \in N(\vec{x}) : \phi(\vec{x}_0) < 0\} \quad (17)$$

The Shi-Karl method avoids directly solving PDE, instead two sets L_{in} and L_{out} are gradually evolved. The evolution is separated into two cycles: data-driven expansion and smoothness regularization with a term derived from a Gaussian filtering process. The first cycle switches grid points from one set L_{in} or L_{out} to another, specified by the sign of the discrete approximation $\hat{F}$ of the speed function, therefore shrinking or expanding the boundary. The regulation cycle provides smoothness regulation to the boundary using local Gaussian filtering. The points during this step are added to one of the sets, depending on the sign of convolution of the level set function with a Gaussian filter. The iteration procedure stops when the stop condition (18) is satisfied or if a pre-specified maximum number of iterations is reached.

$$\hat{F}(\vec{x}) \leq 0, \forall x \in L_{out}, \quad \hat{F}(\vec{x}) \geq 0, \forall x \in L_{in} \quad (18)$$

Those equations disagree with each other on which direction to evolve the boundary only when the energy minimum is reached.

In comparison to other narrowband techniques, the Shi-Karl algorithm performs computation only with two lists of grid points neighboring the surface boundary. Although it belongs to the class of narrowband techniques, representing one of the extreme cases, it has one fundamental difference. The level set curve evolution is done without solving any PDE, thus there is no need for

controlling step size or maintaining numerical stability. Despite avoiding using PDEs, this method preserves all the advantages of the level set: generality of formulations for an arbitrary number of dimensions and automatic handling of topological changes .
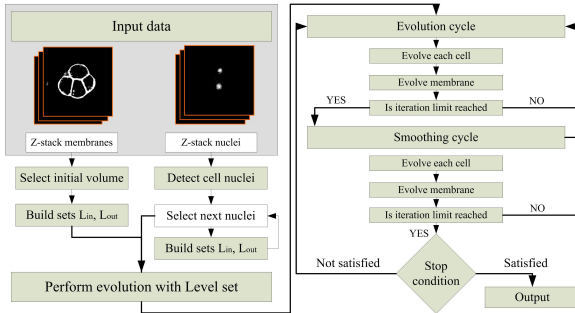

Fig. 9 A scheme of the implemented algorithm. First the sets $L_{i}n$ and $L_{o}ut$ are computed for each inner cell region and membrane. Then the two cycle iterative algorithm is executed.

### 3.2 Experimental results
3.2.1 Dataset

The dataset used in the experiments to test the designed 3D level set method consisted of 20 embryo samples at various development stages (4-32 cells). Female H2B-mCherry mice were crossed with mG mice to obtain embryos, whcih were then recovered and cultured under the condition of 37C, 5% $CO2$ in 20μl drop of KSOM in the chamber installed in the inverted light-sheet microscope. The visual data was composed of 130 optical cross sections, acquired every 10 minutes, the distance between the two consecutive optical slices was 1μm, then scaled to have 260 images. The resolution of the input images was 260x260.

The primary sets L_{in}^{i} and L_{out}^{i} for inner cell regions, used in Shi-Karl iterative algorithm, were initialized with cell nuclei. The nuclei were automatically detected by applying 3D Gaussian filter, followed by Otsu's adaptive thresholding, followed by connected component labeling. Among all detected blobs N with a maximum number of points were chosen. Then the sets were calculated according to their definitions (17). The same approach was applied to determine initial sets of cell membranes (see Figure 9).
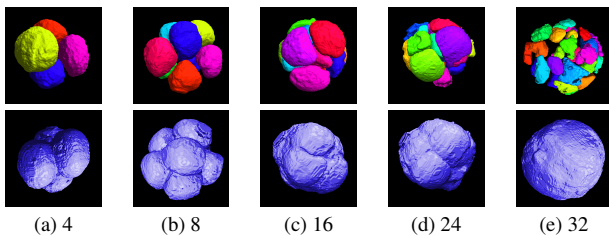
Fig. 10 3D reconstruction of segmentation results for inner cell regions and membranes for embryos containing 4, 8, 16, 24, and 32 cells.

Visual examination of the segmentation results presented on Figure 10 demonstrate that the algorithm was able to correctly identify inner cell regions and membranes for embryos with 4, 8, and 16 cells (see Figure 12). However, if the number of blastomeres was 24 or 32 the algorithm appeared to provide less accurate results. The shapes of the detected inner regions were less

(a) 4   (b) 8   (c) 16   (d) 24   (e) 32
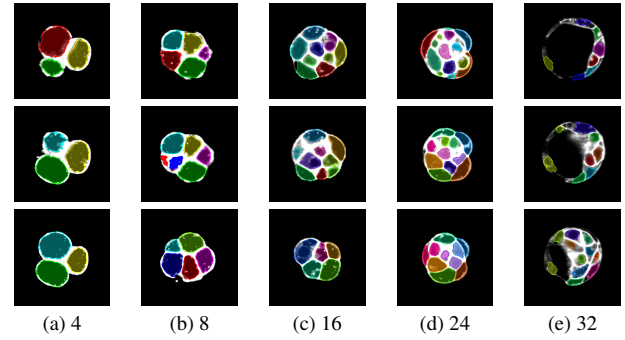
Fig. 11 Cross sections of embryos that contain 4, 8, 16, 24, and 32 blastomeres that display the results of the inner region segmentation with the developed method.

smooth, with traces of under-segmentation. The obtained surface of cell membranes, on the other hand, appeared to suffer less from those problems observed for inner regions.

These results can be explained by the fact that an embryo undergoes a dramatic morphological change that occurs at the 24-32 stage. An internal cavity is formed, forcing blast, forcing blastomeres to clutter to one side of the embryo. The outer membranes, separating the inside and outside environment become less visible, their intensity is low, while the membranes between cells become more prominent.
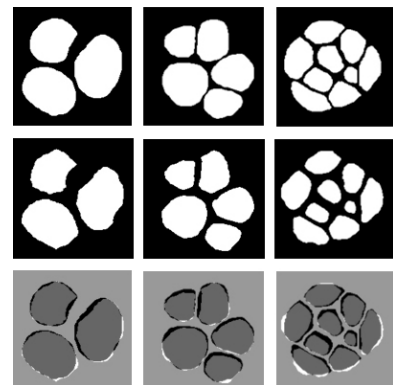
Fig. 12 Top row – ground truth segmentation of inner regions for embryos at 4, 8, 16 cell stages. Middle row – output of theproposed algorithm. Bottom row – error maps of the segmentation.

3.2.2 Quantitative accuracy evaluation

Performing quantitative assessment of the segmentation accuracy for the described task cannot be done straightforward since it is impossible to obtain ground truth labeling for blastomeres and membranes from any direct measurements. Therefore, to conduct tests, the ground truth set was built by manually specifying areas of inner cell regions and membranes on the input images.

The accuracy of the segmentation for each cell component was evaluated as an average F-score, which is defined as the harmonic mean of precision and recall (see Equations (19) and (20)).

$$F = \frac{2 \times precision \times recall}{precision + recall} \qquad (19)$$

If the segmentation result obtained with the proposed method is denoted as S_e and S_0 is the ground truth, then precision and recall are defined as:

$$precision = \frac{|S_e \cap S_0|}{|S_e|} \qquad recall = \frac{|S_e \cap S_0|}{|S_0|} \qquad (20)$$

The results of the segmentation for inner cell regions and membranes given as precision, recall and F-measure are presented in Table 6 and Table 7.

Cell count	4	8	16	24	32
Precision	0.93	0.93	0.85	0.8	0.66
Recall	0.93	0.9	0.9	0.83	0.80
F-score	0.93	0.91	0.88	0.81	0.75

Table 6 Segmentation accuracies for inner cell regions presented as precision, recall, F-score for embryos with different number of blastomeres.

Cell count	4	8	16	24	32
Precision	0.81	0.78	0.7	0.73	0.75
Recall	0.79	0.77	0.74	0.69	0.67
F-score	0.8	0.79	0.72	0.72	0.7

Table 7 Segmentation accuracies for cell membranes presented as precision, recall, F-score for embryos with different number of blastomeres.

The F-measure of labeling inner cell regions is 93% for the 4 cell stage and it gradually dropped as the number of cell increased. For the 32 cell embryos it reached 70%. As it was illustrated above in previous section, this tendency is caused by the increasing embryo's morphological complexity as it undergoes cell division. Segmentation accuracy for the membranes is slightly lower than inner cells, ranging from 70% to 77%, depending on the number of cells.

3.2.3 Comparison with other methods

The segmentation accuracy of the developed method was compared with a conventional 3D watershed algorithm [58]. Initial markers were selected to be cell nuclei that were extracted in the same way as was described for the proposed method. To the input image a Gaussian smoothing was applied, followed by adaptive thresholding. The input images of embryo membranes were thresholded to obtain a binary image, then dilated in order to separate the volume occupied by the embryo cells from the background, then the binary representation of the membrane is subtracted from the images obtained at the previous step.

The implemented watershed method successfully detected some of the cell regions, yet other regions suffered from under-segmentation. The segmentation accuracy for embryos with 4, 8, 16, and 24 blastomeres of the watershed algorithm was lower than the proposed 3D level set method (see Table. 8). For 32 cell embryo, the watershed approach showed slightly better results. However, it has to be noted that this implementation of the watershed unlike the developed level set method allowed detection only of the inner cell region and not designed for reconstructing membranes.

Cell count	4	8	16	24	32
3D level set	0.93	0.91	0.88	0.81	0.75
Watershed	0.73	0.89	0.83	0.78	0.77

Table 8 Comparison of inner cell region segementation accuracy achieved with the developed 3D level set method and watershed method.

The are only a few reports where for a newly proposed method

a numerical assesment of segmentation accuracy is presented. Guisti et al. [42] proposed a method that involves processing of Z-stack of HMC images. They assessed its efficiency on 53 4-cell embryo image stacks. During the testing stage, the candidate cell was considered as correct if its Jaccard similarity index was higher than 0.8, achieving 71% of accuracy. Singh et al. [41] applied isoperimetric graph partitioning to HMC embryo images to approximate blastomere position. It achieved 81% of accuracy (Jaccard similarity index was also set to 0.8) on a dataset of 40 embryo images. In comparison, the approach described in this thesis was able to achieve 90% with the same evaluation technique.

3.2.4 Individual energy terms

Fine-tuning weights in the definition of the energy functions $E_{inner}(\phi_i)$ and $E_{membrane}(\psi)$ is a difficult procedure, since there is no guarantee that the chosen set allows achieving the best accuracy. Thus to understand how the individual energies affect accuracy of segmentation a number of weight sets were tested (see Table 9 and Table 10). The accuracies of blastomere and membrane segmentation were calculated for an embryo with 8 cells.

w_1	w_2	w_3	Accuracy
0	1	1	0.63
1	1	0	0.74
1	1	1	0.90
1	1	3	0.91

Table 9 Accuracy of cell region segmentation depending on weight values for an embryo with 8 cells presented as F-score

v_1	v_2	v_3	Accuracy
1	0	0	0.75
0	1	1	0.77
1	1	1	0.79
1	1	3	0.8

Table 10 Accuracy of membrane segmentation depending on weight values for an embryo with 8 cells presented as F-scores

Exclusion of $E_{volume}(\psi)$ forces to rely only on $E_{inclusion}(\psi)$ during evolution of cell membranes, results in under segmentation.

3.3 Discussion

The use of fluorescence visual data instead of images, obtained with Hoffman Modulation Contrast (HMC) technique greatly facilitates localization of blastomeres and cell membranes.

Experimental results showed that the developed 3D level set algorithm was capable of segmenting efficiently embryos with up to 24 cells. However due to significant changes in internal embryo morphology it did not achieve good results for the samples containing 32 cells. The advantages of the designed 3D level set method include handling complex embryo morphology, restoring regions of membranes with low visibility and processing speed.

There are two factors which primarily affect the segmentation accuracy of the developed method. The first one is the design and usage of the energy term $E_{inclusion}(\psi)$. This energy was created to correctly fill 'holes' by enveloping inner cell regions and in some cases it forces to incorrectly add regions which are not belong to membranes. The second factor, contributing to estimation accuracy, is the precision of Canny detector used for computing

edgeness function $e(x, y, z)$. Re-defining edgeness metric with a different function potentially can increase the accuracy.

Another approach for improving segmentation accuracy, for the 32-cell embryos in particular, is to introduce additional energies into equation (8) and (9). For example, to carry out more direct control of blastomere smoothness an individual smoothness energy can be included into computations, instead of relying on regularization cycle of the Shi-Karl iterative algorithm. Specifying an energy for a cavity in the 32-cell embryo could also increase the result of segmentation.

The implementation of the method was also done as a stand-alone tool with a GUI, that aided visualization of the resultative segmentation (see Figure 13).
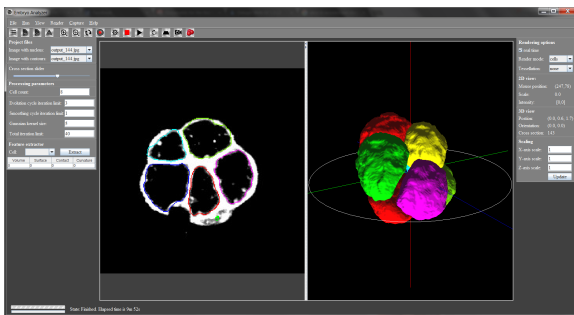

Fig. 13 The 3D level set algorithm for early embryo segmentation was implemented as a stand-alone application with a GUI.

4. Conclusion

The advances in live cell imaging allowed rapid acquisition of high volumes of visual data, dramatically transforming the biomedical science. Image-based experiments became the standardized approach to carry out scientific studies. Significant progress has been achieved in developing new devices and techniques for data acquisition, yet there is still lack of tools that aid to process and analyze obtained data automatically. Image processing frameworks that were primarily designed for generic tasks of image classification or semantic segmentation are often not directly applicable to biomedical problems. Frequent changes in device settings used to obtain images, high variety of input samples, the necessity of achieving high accuracy - all these factors make it challenging to devise a robust approach. Thus a considerable number of studies conducted rely on manual processing of collected data.

Furthermore, even if an algorithm that automatizes the process of biomedical investigation can be developed an assessment of its accuracy presents difficulties. The main reason is that commonly the ground truth, especially in cases of where it is required to execute cell detection or segmentation, cannot be obtained by direct measurements, demanding to reserve to indirect evaluation, qualitative analysis or providing manually prepared ground truth data.

Studies, that were presented in this paper introduced two new methods for computer-aided biomedical image analysis. More specifically, both of the developed methods targeted the most common task that occurs during biomedical research - cell analysis.

The first method was designed in order to aid bacteriologists with the task of DST. In particular, the DST procedure in our studies was carried out with the help of a special microfluidic device - DSTM device, designed to reduce the time necessary to obtain the image of cells grown in presence of a drug with different concentrations. Previously the cell analysis procedure was carried out manually, by visually observing changes in cell growth rate and morphology, examining images of the device captured with a camera attached to a phase contrast microscope. The implementation of the developed algorithm for automatic cell analysis, which was produced as a stand-alone tool, greatly facilitated DST procedure. It allowed efficiently detect cells and extract their features, that can be used later for detailed analysis by a human expert. In addition, it was also capable of determining strain susceptibility and its MIC without any user involvement using classification algorithm based on SVM. The tests, evaluating the accuracy of the built algorithm on a dataset, containing 101 images for each one of 5 drugs, showed high accuracy. The method was able to achieve a 97% accuracy, despite the fact, that a rather straightforward image processing techniques were used. The developed software application has been planned to supply with the device to hospitals, and other medical organizations to facilitate rapid drug testing.

The second method was designed to solve the task of early-stage embryo segmentation into inner cell regions and membranes. Segmentation of embryo into the individual cell would simplify the extraction of cell characteristics. That in its turn would allow building new models of cell specialization process, moving forward the field of transplant medicine and genetic disorder diagnosis. Previously introduced techniques for achieving embryo segmentation used HMC images, that due to the process of acquisition, make it dramatically more complex to obtain correct results for embryos with a high number of cells. On the other hand, fluorescence protein imaging procedure makes it possible to capture images with marked cell components, such as membranes and nuclei. Exploiting this advantage, we proposed a new 3D level set method for embryo segmentation from 2 Z-stacks (cell membrane and nuclei). The 3D level set involves solving PDEs, derived from the definition of energy functions. The energy functions in the proposed methods were designed to take into account intensity levels of cell membranes and internal morphological structure. Instead of solving PDEs directly, an iterative two cycle technique was used, significantly reducing computational burden. To visualize results, and the stand-alone tool was created, utilized to conduct a qualitative and quantitative assessment of the accuracy of the proposed algorithm. The accuracy of the method achieved 93% for 4-cell embryo, gradually reduced with the increase of blastomeres, reaching 75% for 32-cell case.

More and more challenging image analysis tasks are being solved in the biomedical field. Ability to construct automatic systems, capable of providing high level contextual and semantic analysis of images with the same accuracy as a trained expert, or even higher, without doubt will be beneficial to biomedical field.

References

[1] Roland, E. and Chaitanya, A.: Computational imaging in cell biology, *Journ. Cell Biol.*, Vol. 161-3
DOI: 10.1083/jcb.200302097 (2003)

[2] Murphy, R. F., and Meijering, E. and Danuser, G.: Special Issue on Molecular and Cellular Bioimaging, *IEEE Transactions on Image Processing*, Vol.4-9, pp.1233–1236 (2005).

[3] Brinkmann, M., Lutkemeyer, D., Gudermann, F., and Lehmann, J.: New technologies for automated cell counting based on optical image analysis The Cellscreen, *in Proc. of the 17th ESACT Meeting*, Vol.1, pp.269-273
DOI: 10.1007/978-94-010-0369-8_64 (2001)

[4] Zhou, X., Cao, X., Perlman, Z., and Wong, S. T.: A computerized cellular imaging system for high content analysis in monastrol suppressor screens, *J Biomed Inform*, Vol.39, pp.115125

[5] Dufour, A., Shinin, V., Tajbakhsh, S., Guillen-Aghion, N., and Olivo-Marin, J.-C.: Segmenting and tracking fluorescent cells in dynamic 3-D microscopy with coupled active surfaces, *IEEE Signal Processing Society*, Vol.14-9, pp.1396-1410
DOI: 10.1109/TIP.2005.852790 (2005)

[6] Dzyubachyuk, O., A. van Cappellen, W., Essers, J. and J. Nissen, W.: Advanced Level-Set-Based Cell Tracking in Time-Lapse Fluorescence Microscopy, *IEEE Transactions on Medical Imaging*, Vol.29-3, pp.852-867
DOI: 10.1109/TMI.2009.2038693 (2010)

[7] Lee V. C.: The antibiotic resistance crisis: Part 1: Causes and threats. pharmacy and therapeutics, *Pharmacy and Therapeutics*, Vol.40, pp.277283 DOI: 10.3855/jidc.3573 (2015)

[8] Levy, S. B.: Factors impacting on the problem of antibiotic resistance, *J. Antimicrob. Chemother.*, Vo.49, pp.2530
DOI: 10.1093/jac/49.1.25 (2002)

[9] Jorgensen J. H. and Ferraro M. J.: Antimicrobial susceptibility testing: A review of general principles and contemporary practices, *Clin Infect Dis.* Vol. 49 pp. 17491755
DOI: 10.1086/647952 (2009)

[10] Ericsson H. M and Sherris J. C.: Antibiotic sensitivity testing. report of an international collaborative study, *Acta Pathol Microbiol Scand B Microbiol Immunol* (1971)

[11] Huang M. B., Baker C. N., Banerjee S., and Tenover F. C: Accuracy of the e test for determining antimicrobial susceptibilities of staphylococci, enterococci, campylobacter jejuni, and gram-negative bacteria resistant to antimicrobial agents, *J Clin Microbiol*, Vol.30, pp.32438, (1992)

[12] Jorgensen J. H. and Ferraro M. J.: Antimicrobial susceptibility testing: A review of general principles and contemporary practices, *Clin Infect Dis.* , Vol.49, pp.1749 1755, (2009)

[13] Mittman S. A., Huard R. C., Della-Latta P., and Whittier S: Comparison of BD Phoenix to Vitek 2, MicroScan MICroSTREP, and Etest for antimicrobial susceptibility testing of streptococcus pneumoniae, *J Clin Microbiol*, Vol. 47, pp.355761 (2009)

[14] Jungil C., Jungheon Y., Mincheol L., Eun-Geun K., Ji Soo L., Seungok L., Seik J., Sang Hoon S., and et. al.: A rapid antimicrobial susceptibility test based on single-cell morphological analysis, *Science Translational Medicine*, Vol.6, (2014)

[15] Price C. S., Kon S. E., and Metzger S.: Rapid antibiotic susceptibility phenotypic characterization of Staphylococcus aureus using automated microscopy of small numbers of cells, *J Microbiol Methods, Vol.98, pp.50-58,*
DOI: 10.1016/j.mimet.2013.12.021 (2014)

[16] Iino R., Nishino K., Yamaguchi A., Matsumoto Y.: A microfluidic device for simple and rapid evaluation of multidrug efflux pump inhibitors, *Front Microbiol.*, Vol.3-40
DOI: 10.3389/fmicb.2012.00040 (2012)

[17] Matsumoto Y., Hayama K., Sakakihara S., Nishino K., Noji H., Iino R., and Yamaguchi A.: Evaluation of Multidrug Efflux Pump Inhibitors by a New Method Using Microfluidic Channels, *PLoS One*, Vol.6-4
DOI: 10.1371/journal.pone.0018547 (2011)

[18] Carpenter A. E., Jones T. R., Lamprecht M. R., Clarke C., Kang H., et al.: CellProfiler: image analysis software for identifying and quantifying cell phenotypes, *Genome Biology*, Vol.7-100
DOI: 10.1186/gb-2006-7-10-r100 (2006)

[19] Klein, A., Van den Doel, R., Young, I. T., and Van Vliet, L. J.: Quantitative evaluation and comparison of light microscopes, *in Proc. of SPIE The International Society for Optical Engineering* (2012)

[20] Otsu N.: A threshold selection method from gray-level histograms, *IEEE Trans. Systems Man. Cybernet*, Vol.9-1, pp.62-61
DOI: 10.1109/TSMC.1979.4310076 (1979)

[21] Matas J., Galambos, C., Kittler J.: Progressive Probabilistic Hough Transform, *Computer Vision and Image Understanding*, Vol.78-1, pp.119-137
DOI: 10.1006/cviu.1999.0831 (2000)

[22] Whitesides G. M., Ostuni E., Takayama S., Jiang X., Ingber D. E.: Soft Lithography in Biology and Biochemistry, *Annual Review of Biomedical Engineering*, Vol.3, pp.335-373
DOI: 10.1146/annurev.bioeng.3.1.335 (2001)

[23] Matsumoto Y., Sakakihara S., Grushnikov A., Kikuchi K., Noji H., Yamaguchi A., Iino R., Yagi Y., and Nishino K.: A Microfluidic Channel Method for Rapid Drug-Susceptibility Testing of Pseudomonas aeruginosa, *PLoS One*, Vol.11-2
DOI: 10.1371/journal.pone.0148797 (2016)

[24] Qi X., Xing F., Foran J. D., and Yang L.: Robust Segmentation of Overlapping Cells in Histopathology Specimens Using Parallel Seed Detection and Repulsive Level Set *IEEE Trans. Biomed Eng.*, Vol.59-3, pp.754-765
DOI: 10.1109/TBME.2011.2179298 (2012)

[25] Samet H. and Tamminen M.: Efficient Component Labeling of Images of Arbitrary Dimension Represented by Linear Bintrees, *IEEE Trans. PAMI*, Vol.10-4, pp.579
DOI: 10.1109/34.3918 (1988)

[26] Zhang T. Y., Suen C. Y.: A fast parallel algorithm for thinning digital patterns, *Communications of the ACM*, Vol.27-3, pp.236-239
DOI: 10.1145/357994.358023 (1984)

[27] Burges, Christopher J.C.: A Tutorial on Support Vector Machines for Pattern Recognition *Data Mining and Knowledge Discovery*, Vol.2-2, pp.121-167
DOI: 10.1023/A:1009715923555 (1998)

[28] Wahba G.: Support Vector Machines, Reproducing Kernel Hilbert Spaces and the Randomized GACV, *in Proc. of the 1997 NIPS Workshop on Support Vector Machines*,
DOI: 10.1.1.53.2114

[29] Choi J., Yoo J., Lee M., Kim E-G., Lee J. S., Lee S., Joo S., et. al.: A rapid antimicrobial susceptibility test based on single-cell morphological analysis, *Science Translational Medicine* , Vol.6-267,
DOI: 10.1126/scitranslmed.3009650 (2014)

[30] Chen C. H., Lu Y., Sin M. L., Mach K., Zhang D., Gau V., Liao J. C., Wong P. K.: Antimicrobial Susceptibility Testing Using High Surface-to-Volume Ratio Microchannels, *Analytical Chemistry*, Vol.82-3, pp.1012-1019,
DOI: 10.1021/ac9022764 (2010)

[31] Kalashnikov M., Lee J. C., Campbell J., Sharon A., Sauer-Budge A. F.: A microfluidic platform for rapid, stress-induced antibiotic susceptibility testing of Staphylococcus aureus, *Lab Chip.*, Vol.12-12, pp.4523-4532,
DOI: 10.1039/c2lc40531h (2012)

[32] Price C. S., Kon S. E., Metzger S.: Rapid antibiotic susceptibility phenotypic characterization of Staphylococcus aureus using automated microscopy of small numbers of cells, *J Microbiol Methods*, Vol.98, pp.50-58,
DOI: 10.1016/j.mimet.2013.12.021 (2014)

[33] Grushnikov A., Kikuchi K., Matsumoto Y., Kanade T., Yagi Y.: Automatic Image Analysis for Rapid Drug Susceptibility Testing, *Advanced Biomedical Engineering*, Vol.6, pp.76-82,
DOI: 10.14326/abe.6.76 (2017)

[34] Bedzhov I., Graham S. J., Leung C. Y., Zernicka-Goetz M.: Developmental plasticity, cell fate specification and morphogenesis in the early mouse embryo, *Philosophical Transactions of the Royal Society of London B: Biological Sciences*, Vol.369-1657,
DOI: 10.1098/rstb.2013.0538 (2014)

[35] Zernicka-Goetz M., Morris S. A., Bruce A. W.: Making a firm decision: multifaceted regulation of cell fate in the early mouse embryo, *Nature Reviews Genetics*, Vol.10, pp.467-477,
DOI: 10.1038/nrg2564 (2009)

[36] Rossant J. and Tam P.L.: Emerging asymmetry and embryonic patterning in early mouse development, *Dev. Cell*, Vol.7-2, pp.155-164,
DOI: 10.1016/j.devcel.2004.07.012 (2004)

[37] Tarkowski A. K. and Wróblewska J.: Development of blastomeres of mouse eggs isolated at the 4- and 8-cell stage, *Development*, Vol.18-1, pp.155-180 (1967)

[38] Wennekamp S., Mesecke S., Nedelec F., Hiiragi T.: A self-organization framework for symmetry breaking in the mammalian embryo, *Nature Reviews Molecular Cell Biology*, Vol.14, pp.452-459
DOI: 10.1038/nrm3602 (2013)

[39] Dard N., Louvet-Valle S., Maro B.: Orientation of Mitotic Spindles during the 8- to 16-Cell Stage Transition in Mouse Embryos, *PLoS ONE*, Vol.4-12, pp.1-8
DOI: 10.1371/journal.pone.0008171 (2009)

[40] Stephenson R. O., Yamanaka Y., Rossant J.: Disorganized epithelial polarity and excess trophectoderm cell fate in preimplantation embryos lacking E-cadherin, *Development*, Vol.137-20, pp.3383-3391
DOI: 10.1242/dev.050195 (2010)

[41] Singh A., Buonassisi J., Saeedi P., and Havelock J.: Automatic blastomere detection in day 1 to day 2 human embryo images using partitioned graphs and ellipsoids, *in Proc. Image Processing (ICIP), 2014 IEEE International Conference on*
DOI: 10.1109/ICIP.2014.7025184 (2014)

[42] Giusti A., Corani G., Gambardella L., Magli C., Gianaroli L.: Blastomere segmentation and 3D morphology measurements of early embryos from Hoffman Modulation Contrast image stacks, *in Proc. Biomedical Imaging: From Nano to Macro, 2010 IEEE International Symposium on*
DOI: 10.1109/ISBI.2010.5490225, (2010)

[43] Al-Kofahi Y., Lassoued W., Lee W., Roysam B.: Improved automatic detection and segmentation of cell nuclei in histopathology images, *IEEE Trans Biomed Eng*, Vol.57-4, pp.841-52,
DOI: 10.1109/TBME.2009.2035102, (2010)

[44] Ortiz De Solorzano C., Malladi R., Lelivre S. A., Lockett S. J.: Segmentation of nuclei and cells using membrane related protein markers, *Journal of Microscopy*, Vol.201-3, pp.404-415,
DOI: 10.1046/j.1365-2818.2001.00854.x (2001)

[45] Fernandez R., Das P., Mirabet V., Moscardi E., Traas J., Verdeil J.-L., Malandain G., Godin C.: Imaging plant growth in 4D: robust tissue reconstruction and lineaging at cell resolution, *Nat Meth*, Vol.7-7, pp.547-553,
DOI: 10.1038/nmeth.1472 (2001)

[46] Tian Y., Yin Y., Duan F., Wang W., Wang W., Zhou M.: Automatic blastomere recognition from a single embryo image, *Comput Math Methods Med*
DOI: 10.1155/2014/628312 (2014)

[47] Nowotschin S., Eakin G. S., Hadjantonakis A.-K.: Live-imaging fluorescent proteins in mouse embryos: Multi-dimensional, multi-spectral perspectives, *Trends Biotechnol.*, Vol.27-5, pp.266-267
DOI: 10.1016/j.tibtech.2009.02.006 (2009)

[48] Xinghua L., Minjung K., Munoz-Descalzo S., Hadjantonakis A.-K.: A Rapid and Efficient 2D/3D Nuclear Segmentation Method for Analysis of Early Mouse Embryo and Stem Cell Image Data, *Stem Cell Reports*, Vol.11, pp.382-397
DOI: 10.1016/j.stemcr.2014.01.010 (2014)

[49] Mandar M. D., Bosiljka T., Kazunari M., Ling L., Liqun L.: A Global Double-Fluorescent Cre Reporter Mouse, *Genesis*, Vol.45-9, pp.593-605 (2007)

[50] Grushnikov A., Niwayama R., Kanade T., Yagi Y.: 3D level set method for blastomere segmentation of preimplantation embryos in fluorescence microscopy images *Machine Vision and Applications*, pp.1-11, DOI: 10.1007/s00138-017-0880-0 (2017)

[51] Kass M., Witkin A., Terzopoulos D.: Snakes: Active contour models, *International Journal of Computer Vision*, Vol.1-4, pp.321-331,
DOI: 10.1007/BF00133570 (1988)

[52] Cohen L. D., Cohen I.: A finite element method applied to new active contour models and 3D reconstruction from cross sections, *Proceedings Third International Conference on Computer Vision* DOI: 10.1109/ICCV.1990.139601 (1990)

[53] Lefohn A. E., Kniss J. M., Hansen C. D., Whitaker R. T.: A streaming narrow-band algorithm: Interactive computation and visualization of level sets, *IEEE Trans. on Visualization and Computer Graphics*, Vol.10-4, pp.422-433
DOI: 10.1109/TVCG.2004.2 (2004)

[54] Osher S., and Sethian J. A.: Fronts propagating with curvature dependent speed: algorithms based on Hamilton-Jacobi formulations, *Journal of Computational Physics*, Vol.79-1, pp.12-49
DOI: 10.1016/0021-9991(88)90002-2 (1988)

[55] Shi Y. and Karl W. C.: A real-time algorithm for the approximation of level-aet-based curve evolution, *IEEE Trans Image Process.*, Vol.17-5, pp.645-656
DOI: doi:10.1109/TIP.2008.920737 (2008)

[56] Brox T. and Weickert J.: Level Set Segmentation With Multiple Regions, *IEEE Trans. on Image Processing*, Vol.15-10, pp.3213-3218
DOI: 10.1109/TIP.2006.877481 (2006)

[57] Adalsteinsson D. and Sethian J. A.: A Fast Level Set Method for Propagating Interfaces, *Journal of Computational Physics*, Vol.118, pp.269-277
DOI: 10.1006/jcph.1995.1098 (1995)

[58] Malpica N., de Solrzano C. O., Vaquero J. J., Santos A., Vallcorba I., Garca-Sagredo J. M., del Pozo F.: Applying watershed algorithms to the segmentation of clustered nuclei, *Cytometry*, Vol.28-4,
DOI: 10.1002/(SICI)1097-0320(19970801)28:4¡289::AID-CYTO3¿3.0.CO;2-7 (1997)